Effects of Cl+ and F+ implantation of oxidation-induced stacking faults in silicon

Xu, J. Y.; Bronsveld, P. M.; Boom, G.; de Hosson, J. Th. M.

Published in:
Journal of Applied Physics

DOI:
10.1063/1.332958

Publication date:
1984

Effects of Cl^+ and F^+ implantation of oxidation-induced stacking faults in silicon

J. Y. Xu,[a] P. M. Bronsveld, G. Boom, and J. Th. M. De Hosson
Department of Applied Physics, Material Science Centre, University of Groningen, Nijenborgh 18, 9747 AG Groningen, The Netherlands

(Received 1 August 1983; accepted for publication 9 January 1984)

Three implantation effects were investigated in floating-zone-grown silicon: (a) the effect of Cl^+ implantation resulting in the shrinkage of oxidation-induced stacking faults; (b) the effect of F^+ implantation giving rise to defaulting of the 1/3[111] Frank dislocations into 1/2[110] perfect dislocations due to the interaction with 1/6[11$\bar{2}$] Shockley partials; (c) the effect of a combined F^+ and Cl^+ implantation of dislocation motion. Notwithstanding the limited magnification of double-crystal x-ray topography it proves to be a valuable technique for determination of the effects of implantation, as removal of *F*; the oxidation layer is unnecessary for observation of the oxidation-induced stacking faults. Moreover, the role of the oxide layer in the Si-SiO_2 interface can be followed more appropriately.

PACS numbers: 61.70.Ph, 61.70.Tm, 61.70. Le, 81.60. – j

I. INTRODUCTION

Oxidation is an inevitable accompaniement in the fabrication of almost every silicon integrated circuit device. As a consequence, crystallographic defects are frequently generated. In particular, the presence of oxidation-induced stacking faults (OSF) have a deleterious effect on the electrical performance of bipolar charge-coupled imaging devices.

The effect of Cl^+ and F^+ ion implanatation of oxidation-induced stacking faults in floating-zone-grown (FZ) silicon was investigated using double-crystal x-ray topography. In one sense, this research is a continuation of the work by Kawado,[1] who implanted Czochralski-grown silicon with 10^{14}–10^{16} Cl^+ ions/cm^2 of 200 keV. He reported both on shrinkage and unfaulting of existing stacking faults, measured by optical and electron microsopy. In another sense, this research is a continuation of the work by Patel and Authier[2] who studied defects in silicon by x-ray topography permitting them to study stacking faults *in situ* without removal of the oxide layer. The ongoing controversy on the role of interstitials or vacancies in the shrinkage process is most recently described by Tan and Gösele.[3]

II. EXPERIMENTAL METHODS

Silicon wafers (Wacker, West Germany) of 280 μm in thickness and a [001] surface normal, cut from FZ crystals, were used. The wafers were *n* type (P doped) with a specific resistance of 1–2.5 Ω cm. They were cleaned by a standard procedure of sequential steps of degreasing, scrubbing, chemical cleaning with xylene, HNO_3, and HF, and a deionized water rinse of several minutes prior to drying.

Stacking faults were nucleated by oxidizing wafers in a dry, 0.1-MPa oxygen atmosphere at 1473 K for 130 min. After removal of the oxide layer with a 48% aqueous solution of HF the size of a few carefully selected stacking faults was measured. A first set of wafers was oxidized anew, now at 1423 K for varying periods of time. The increase of the OSF size was determined as a function of oxidation time. The measurements were done by light microscopy, so the oxide layer had to be removed after each treatment, and the surface etched[4] to reveal the OSF intersecting the surface.

Another wafer was oxidized at 1423 K in 0.1-MPa dry oxygen for 25 h. 10^{16} Cl^+ ions/cm^2 of 100 keV were implanted in the oxide layer. The projected range of these ions in SiO_2 is 87 nm while the oxide layer is about 500 nm thick (see Ref. 5). X-ray topographs were taken without removal of the oxide layer. Again the size of a few carefully selected stacking faults was measured and their shrinkage followed as a function of annealing time in dry 0.1-MPa oxygen at 1473 K. The growth rate of the oxide layer during this annealing is 400 nm/h.

Yet another wafer was oxidized, at 1423 K for 4 h in 0.1-MPa dry oxygen, and various sizes of stacking faults were observed by light microscopy on the Wright Jenkins[4] etched surface of the wafer. Four groups of stacking faults on the four possible {111} planes were selected for x-ray topography. Subsequently, the wafer was oxidized in 0.1-MPa dry oxygen at 1473 K for 20 min in order to grow a film of SiO_2 about 130 nm thick. Then 10^{17} ions cm^2 25 keV F^+ was implanted in this layer. The projected range of F^+ in the oxide layer is 40 nm.[5]

As the stacking fault depth in the case of the shrinkage experiment was only small in comparison with the total wafer thickness, a double-crystal back-reflection setup (Bragg case) was built (Fig. 1). Cu$K\alpha_1$ radiation was used with a μd value of 2.8. The first crystal was a dislocation-free silicon wafer with a [001] surface-normal set in a 004 reflection condition. The sample crystal also with a [001] surface normal was set in a 2$\bar{2}$4 reflection condition. The angle between the surface of the second crystal and the beam incident on that surface was 9 deg. As a result the diffracted beam was rather wide, so that section topography could be used. That means that no scanning is usually necessary over a larger area of the sample than is already fulfilling the Bragg condition in the initial, fixed, position at the start. Due to the oxidation and implantation, the sample was rather curved, thus reducing

[a] On leave of absence from Shanghai Institute of Metallurgy, Academia Sinica, The People's Republic of China.

 0021-8979/84/103485-05$02.40

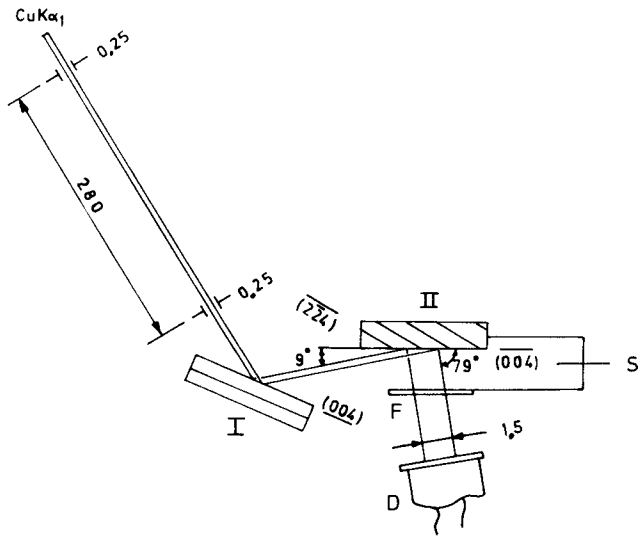

FIG. 1. Double-crystal x-ray ($n, -m$) topography. I: First crystal; II: sample; F: film; D: detector; S: scanning table.

the area over which reflection occurred. Because of the asymmetric setting (Fig. 1) it was still feasible to have a section topograph of 1.5×12 mm^2. With Cu$K\alpha_1$ radiation from a tube run at 38 kV and 18 mA using spot focus (0.4×0.8 mm^2) a 5-h exposure time on Agfa D4 was sufficient. This film has a 0.55-μm grain size. Only one layer of the doubly coated film was used.

For determination of the displacement vector of the stacking faults and the Burgers vector of the accompanying dislocations, both reflection and transmission topography were used. In the latter case the beam is entering from the back of the wafer and leaving through the surface with the oxide layer. In such a setup the diffracted beam is very narrow so that it is necessary to make a scanning-transmission topograph. The area scanned was 4×12 mm^2; the exposure time is 60 h on Agfa D7. This film has a grain size of 0.88 μm; again, only one side of the doubly coated film was developed for higher resolution.

The interference fringes of the $\{111\}$ stacking faults could best be observed in a transmission-section topograph, with Mo$K\alpha_1$ radiation, provided the deviation from the Bragg angle is minimal. The absorption factor is only $\mu d = 0.3$ as compared with $\mu d = 2.8$ in the case of Cu$K\alpha_1$ at the Bragg setting. A transmission-scanning topograph is not quite as clear, because of the overlapping effect during the scanning of dynamical images of different areas shifted in time but reaching the same location on the film. Thirdly, the Mo$K\alpha_1$ extinction distance is 38 as compared to 19 μm for the Cu$K\alpha_1$ case. One disadvantage of Mo$K\alpha_1$ is the low diffracted intensity. Using 38 kV and 18 mA, exposure times of 15 h on Agfa D4 film were required for one section topograph. (On Kodak S0645, used later, 2 h sufficed.)

III. RESULTS AND DISCUSSION

In Fig. 2 several Wright Jenkins etched OSF's are shown imaged in light microscopy. From such photographs the increase in stacking fault size as a function of oxidation

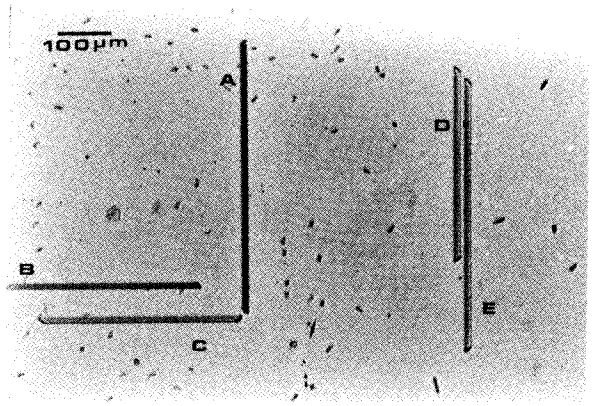

FIG. 2. Light micrograph of several Wright Jenkins' etched OSF's annealed at 1423 K for 230 h in a 0.1- MPa dry oxygen atmosphere.

time was plotted (Fig. 3). It was defined as the fault length on the wafer surface. The error bars are due to the averaging of all appearing sizes on pictures like Fig. 2. The result is in line with the work of Hu,[6] the only difference being that we extended the oxidation time from 10 to 230 h, resulting in stacking faults as large as 500 μm. In Fig. 4 the decrease in size of these stacking faults is plotted as a function of annealing time after implantation of Cl^+. They were measured by x-ray topography. A least-squares fit of Fig. 4 indicates a shrinkage of 21 μm/h for the intersection line of the stacking fault with the etched surface, in agreement with the 22 μm/h reported by Kawado.[1] We did not use the concept of radius since the topographs show that the stacking faults do not have a semicircular shape. Scanning electron microscopy (SEM) data obtained during an earlier study[7] are also plotted in Fig. 4. The initial size was much smaller due to a much shorter oxidation time (2 h at 1473 K). The similarity in slopes indicates that the removal of the oxide layer during the SEM measurements had no effect upon the stacking

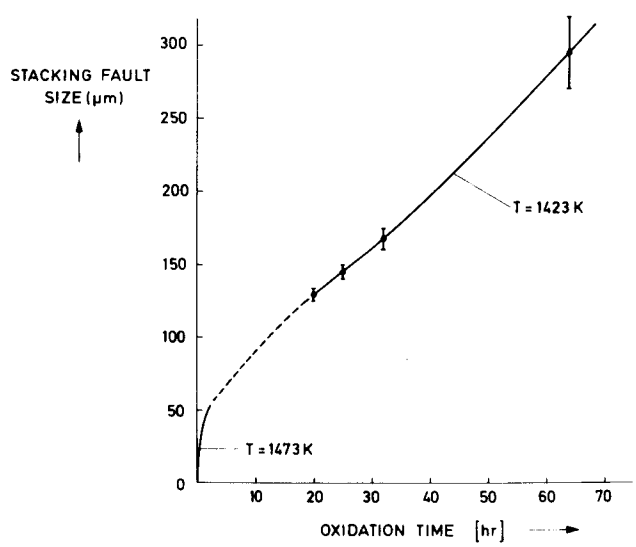

FIG. 3. Increase of stacking fault size vs oxidation time measured with light microscopy.

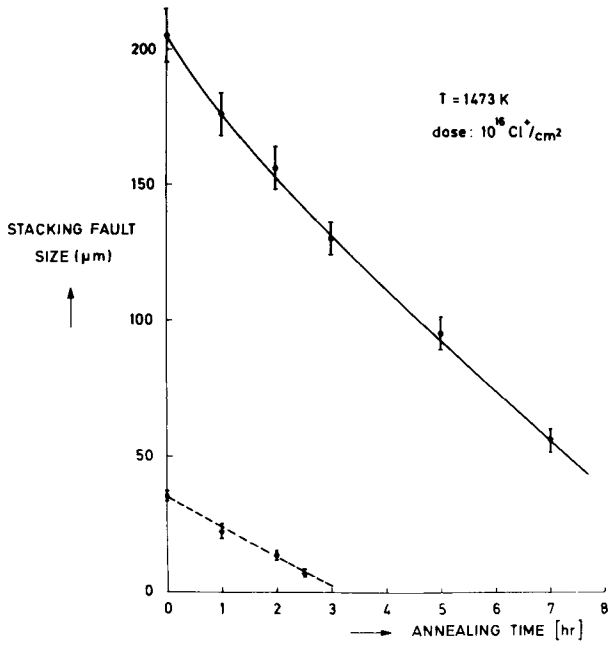

FIG. 4. Decrease of stacking fault size vs annealing time after implantation with Cl^+ ions. Solid line: x-ray topography; dashed line: SEM.[7]

faults. The stacking faults are mostly of the extrinsic type with a 1/3 [111] Frank dislocation at the border (see Maher, Staudinger and Patel).[8] An example of such a stacking fault is given in Fig. 5(a) which is a bright field transmission electron micrograph. In Fig. 5(b) a dark field transmission electron micrograph is depicted. At 100 kV the extinction distance in silicon for the $20\bar{2}$ diffraction factor is 76 nm, so that the sample thickness can be calculated from the number of fringes as being 680 nm. The stacking fault runs from the left being the site of nucleation of the stacking fault to the beam exit surface on the right side.

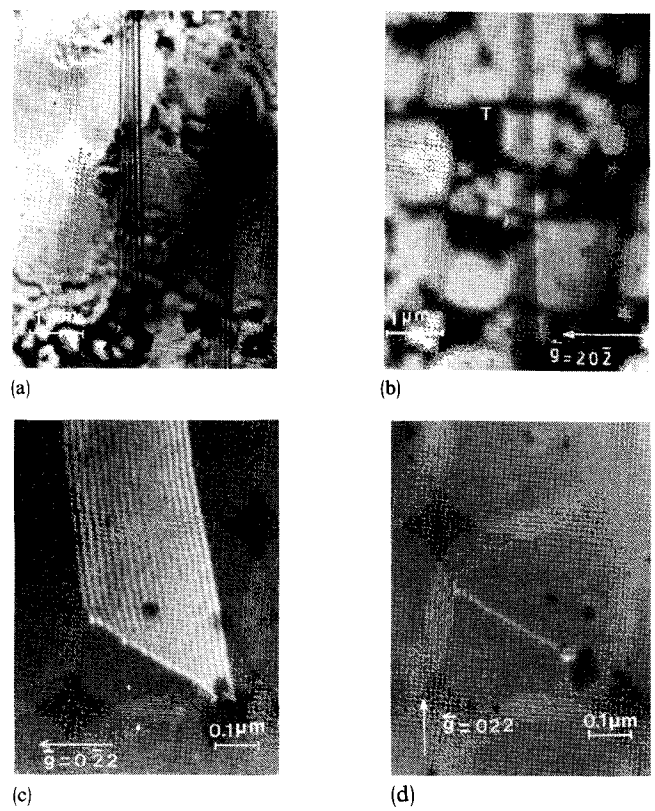

FIG. 5. 100-kV TEM micrographs of several stacking faults: (a) bright field (extrinsic fault); (b) dark field (T = top) ([010](20$\bar{2}$), $b = 1/3[\bar{1}\bar{1}1]$); (c) dark field ([100](0$\bar{2}$2), $s_g > 0$); (d) weak beam/dark field ([2$\bar{1}$1] (022), $s_{g<0}$, Frank partial).

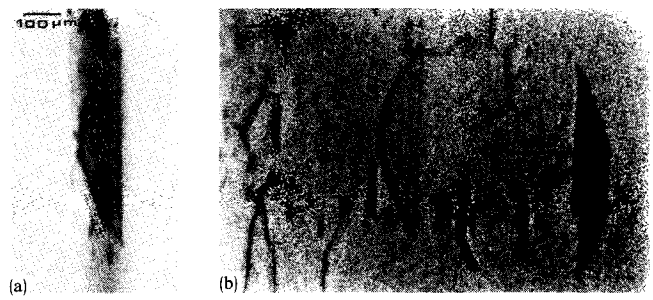

FIG. 6. Mo$K\alpha(n, -m)$ topograph: (a) section, (b) scanning. The first crystal was in (111) and the second in ($\bar{2}$20) setting. The area is the same one as depicted in Fig. 2.

The determination of the stacking fault nature (extrinsic or intrinsic) requires an evaluation of the sense of the displacement vector of the stacking fault $\mathbf{R}_f$. The contrast (black or white) of the outermost fringes relative to the background is determined by the phase shift $2\pi\mathbf{g}\cdot\mathbf{R}_f$ introduced by the stacking fault. From image calculations based on the dynamical theory of electron diffraction,[9] we conclude that the stacking faults imaged in Fig. 5 are extrinsic in nature. The micrographs [Figs. 5(b) and 5(c)] are dark field images. The field-weak beam image [Fig. 5(d)] for a $\mathbf{g}\cdot\mathbf{b}$ analysis of the imperfect dislocation clearly shows that a Frank dislocation bounding the stacking fault is present.

The x-ray topographic result is shown in Figs. 6(a) and 6(b). This is an $(n, -m)$ double-crystal section topograph in which n stands for a 111 reflection and m for a $\bar{2}20$ reflection. The radiation used was Mo$K\alpha_1$, the thickness of the sample 0.2 mm giving an absorption factor of $\mu d = 0.3$. The extinction distance for Mo$K\alpha_1$ radiation in silicon with a $\bar{2}20$ reflection is 38 μm and the depth of the stacking fault is 150 μm. The stacking faults are the same ones as depicted in Fig. 2.

The situation is completely different after implantation

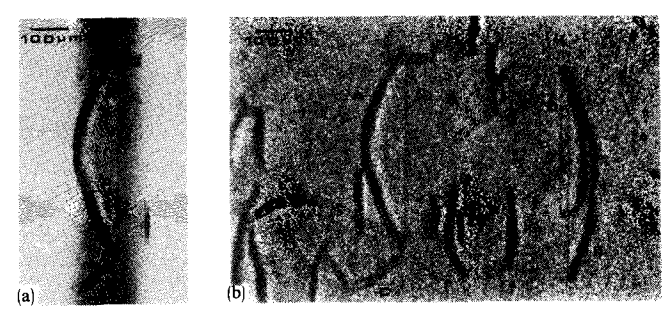

FIG. 7. As in Fig. 6 but after F^+ implantation and a 15-min anneal at 1273 K in a 0.1-MPa dry N_2 atmosphere; (a) section, (b) scanning. Note that the dislocations at B and C on Figs. 2 and 7(b) are not visible on Fig. 6(b) and that the SF fringes in A, D, and E are not present.

TABLE I. Visibility table to determine the Burgers vector of the dislocations before and after implantation.

Defect	Treatment	Diffraction vector used $\bar{2}24$	$2\bar{2}4$	$1\bar{1}1$	$2\bar{2}0$	224	220	Burgers vector	Defect plane	Shape anisotropy	Mechanism
A	Oxidation only	...	no	...	...	...	...	$\frac{1}{3}[\bar{1}11]$	$(\bar{1}11)$	[110]	$\frac{1}{6}[\bar{1}1\bar{2}]+\frac{1}{3}[\bar{1}11]=\frac{1}{2}[\bar{1}10]$
	Oxidation and F^+	...	yes	yes	yes	no partly	no partly	$\frac{1}{2}[\bar{1}10]$	$(\bar{1}11)$	[110]	
B	Oxidation only	...	...	...	...	yes	...	$\frac{1}{3}[111]$	(111)	$[1\bar{1}0]$	$\frac{1}{6}[11\bar{2}]+\frac{1}{3}[111]=\frac{1}{2}[110]$
	Oxidation and F^+	...	no	no	no	yes	yes	$\frac{1}{2}[110]$	(111)	$[1\bar{1}0]$	
C	Oxidation	...	...	...	...	no	...	$\frac{1}{3}[11\bar{1}]$	$(11\bar{1})$	$[1\bar{1}0]$	$\frac{1}{6}[112]+\frac{1}{3}[11\bar{1}]=[110]$
	Oxidation and F^+	...	no	no	no	yes	yes	$\frac{1}{2}[110]$	$(11\bar{1})$	$[1\bar{1}0]$	
D and E	Oxidation only	no	yes	...	...	...	...	$\frac{1}{3}[1\bar{1}1]$	$(1\bar{1}1)$	[110]	$\frac{1}{6}[1\bar{1}\bar{2}]+\frac{1}{3}[1\bar{1}1]=\frac{1}{2}[1\bar{1}0]$
	Oxidation and F^+	yes	yes	yes	yes	no	no	$\frac{1}{2}[1\bar{1}0]$			

with F^+. Perfect dislocation loops are formed out of the stacking faults bounded by Frank partial dislocations because no stacking-fault fringe constrast could be observed in Figs. 7(a) and 7(b), where again the same area is taken. A reaction[10] has taken place according to the equation

$$1/6[11\bar{2}] + 1/3[111] \rightarrow 1/2[110]$$

in the $(\bar{1}10)$ plane. For the set of stacking faults indicated in Figs. 6 and 7 a visibility table (Table I), was set up before and after implanting F^+. Agreement with the work by Salisbury[11] is obtained, although we have not looked for more intricate reaction products such as a $1/6\langle 114\rangle$ component.

The dislocation reaction will only occur when the stacking fault energy is sufficiently high. In the absence of external or internal stresses, and in the absence of thermal energy fluctuations the only force tending to create the Shockley partial (b_p) is due to the stacking fault energy in the Frank loop which produces a force of γ. According to Cottrell[12] the homogeneous nucleation of a Shockley partial requires a shear stress of about $\tau_N = 1.88\times 10^9$ N/m^2. Therefore, spontaneous removal of the fault will occur providing that the stacking fault energy γ is larger than $\tau_N b_p = \simeq 417$ mJ/m^2. Because the actual stacking fault energy is much smaller,[13] homogeneous nucleation is not likely to occur. However, the very large stress τ_N is required only under the extreme condition that the crystal is free from any defect. Local stresses acting in the crystal due to stacking faults present will lower τ_N. In this respect the two implants are behaving differently: Cl^+ stays at the Si–SiO_2 interface and in a reaction with Si produces vacancies with which the Si-self-interstitials can recombine so that the OSF's shrink. Cl^+ is believed to influence indirectly via the interface SiO_2/Si the chemical driving force causing changes in the fault dimensions. However, F^+ diffuses through the Si interstitially maybe preferentially towards the stacking faults causing the unfaulting reaction when high enough in number to create a shear Shockley partial dislocation.

In order to further investigate the microprocesses governing growth and shrinkage of stacking faults we implanted the F^+ sample again, now with Cl^+. The result is given of an additional annealing treatment first in N_2 then in O_2 on the ($F^+ + Cl^+$) sample as well as on the (F^+) sample. Evidently the ($F^+ + Cl^+$) sample in Figs. 8(a) and 8(b) is not showing any change in dislocation length as a function of heat treatment while the original (F^+) sample shows a considerable change in dislocation length at least for the heat treatment in O_2, as can be judged from Figs. 9(a) and 9(b). It is also obvious

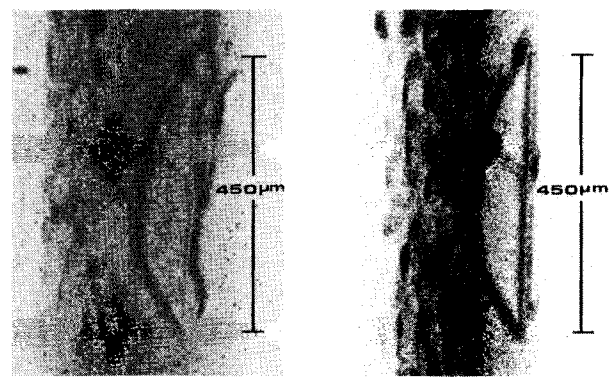

FIG. 8. Effect of annealing in O_2 on a similar dislocation loop as A in Fig. 7 but with an extra Cl^+ implantation: (a) no O_2 anneal, (b) O_2 anneal at 1473 K for 14 h. Note that the dislocation loop measures 450 μm both in (a) and in (b) and nucleation of new defects near the Cl^+ implanted surface is suppressed.

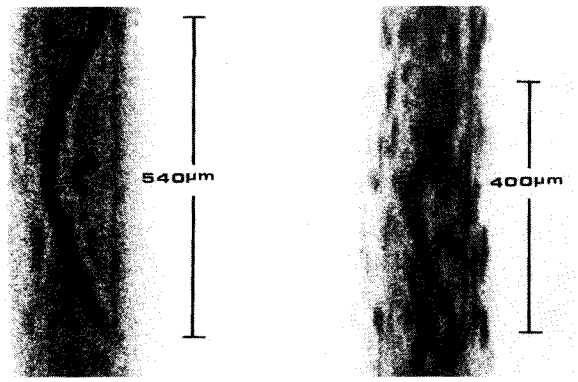

FIG. 9. Effect of annealing in O_2 on dislocation loop A with $b = 1/2[1\bar{1}0]$ after further annealing in N_2 at 1473 K for 2 h and at 1500 K for 10 h without a measurable effect: (a) O_2 anneal at 1473 K for 1/2 h, (b) O_2 anneal at 1473 K for 14 h. Note that the shrinkage from 540 to 400 μm between (a) and (b) and the nucleation of new defects in (b).

from the change in shape of the dislocation line that the dislocation is pinned at the surface. After removal of an additional surface layer of 10 μm by etching, followed by a new heat treatment, the dislocation disappeared.

IV. CONCLUSION

It is possible to use Cl^+ ion implantation (100 keV, 10^{16} ions/cm^2) followed by an annealing treatment for removal of oxidation-induced stacking faults. Judging from the stereo electronmicrographs in Figs. 10(a) and 10(b) the actual shrinkage process should be studied in more detail. With F^+ ion implantation (25 keV, 10^{17} ions/cm^2) we observed a process of unfaulting of the stacking fault with a bordering Frank dislocation changing into a perfect dislocation of type $1/2\langle 110\rangle$. A Shockley partial dislocation should be present to initiate the unfaulting process and, judging from the stereo electronmicrographs in Figs. 11(a) and 11(b), it looks as if this process may start anywhere; however, more detailed study is also required. Subsequent annealing in N_2 did not change either the position or the shape of the perfect dislocation as can be verified by comparing Fig. 9(a) with Fig. 7(a) or 7(b). However, annealing in O_2 resulted in a shortening [Fig. 9(b)], thereby reducing its line tension. Since this perfect dislocation is in part sessile, this part can only climb out of the silicon into the interface by production of vacancies or the absorption of interstitials. Oxidation always produces extra interstitials into the silicon, as is obvious from Fig. 9(b), where quite a number of newly developed stacking faults are visible. In comparison, Fig. 8(b) shows that an extra Cl^+ implantation after the F^+ implantation suppresses these new defects: but at the same time the extra vacancies due to the Cl^+ treatment absorb the interstitials needed for climb of the dislocation and this may explain why now the dislocation did not move at all, neither under a N_2 nor an O_2 treatment.

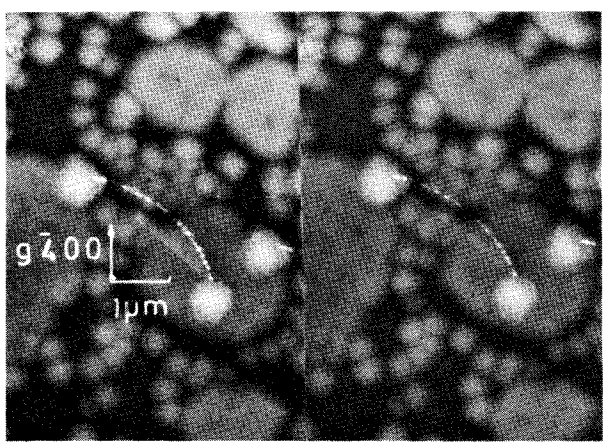

FIG. 10. Stereo-TEM micrographs [010] ($\bar{4}00$) of an OSF with a typical Cl^+ implantation effect. The OSF shrinks while maintaining its shape.

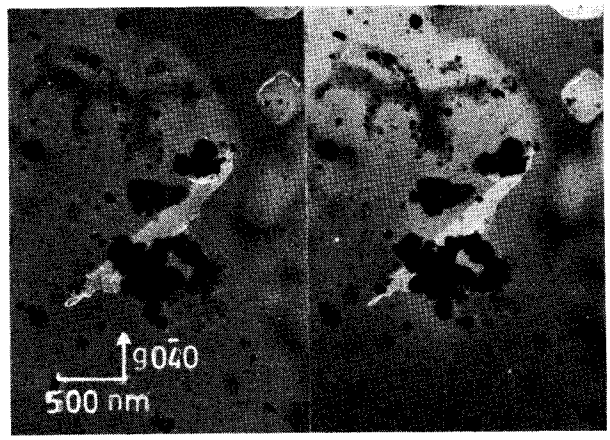

FIG. 11. Stereo-TEM micrographs [100] ($0\bar{4}0$) of an OSF with a typical F^+ implantation effect. Annihilation by interaction with $\langle 112\rangle$ partial dislocations.

ACKNOWLEDGMENTS

The authors would like to thank S. Bakker, H. J. Bron, J. Harkema, M. Mulder, and U. B. Nieborg for their technical assistance. The work was carried out as part of the scientific exchange program between the Royal Netherlands Academy of Arts and Sciences (Amsterdam) and the Academia Sinica of the Peoples's Republic of China. Part of the work reported comes within the scheme of research of the Foundation for Fundamental Research on Matter (F.O.M.-Utrecht) and was made possible by financial support from the Netherlands Organization for the Advancement of Pure Research (Z.W.O.-The Hague).

[1]S. Kawado, Jpn. J. Appl. Phys. **18**, 225 (1979).
[2]J. R. Patel and A. Authier, J. Appl. Phys. **46**, 118 (1975).
[3]T.Y. Tan and U. Gösele, J. Appl. Phys. **53**, 4767 (1982).
[4]Margareth Wright Jenkins, J. Electrochem. Soc. 124, 757 (1977).
[5]J. F. Gibbons, W. S. Johnson, and S. W. Mylroie, *Projected Range Statistics*, 2nd ed. (Dowden, Hutchinson and Ross, Pennsylvania, 1975).
[6]S. M. Hu, Appl. Phys. Lett. **27**, 15 (1975).
[7]P. van Hasselt, J. Th. M. De Hosson, J. Snijder, J. Verwey, Proceedings of the 10th International Congress on Electron Microscopy, Hamburg 2, 387 (1982).
[8]D. M. Maher, A. Staudinger, and J. R. Patel, J. Appl. Phys. **47**, 3813 (1976).
[9]M. J. Whelan, in *Diffraction and Imaging Techniques in Materials Science*, edited by S. Amelinckx, R. Gevers, and J. van Landuyt (North-Holland, Amsterdam, 178), p. 43.
[10]J. A. Lambert and P. S. Dobson, Philos. Mag. **44**, 1043 (1981).
[11]I. G. Salisbury, Acta Metall. **30**, 627 (1982).
[12]A. H. Cottrell, *Dislocations and Plastic Flow in Crystals* (Clarendon, Oxford, 1956).
[13]E. Aerts, P. Delavignette, R. Siems, and S. Amelinckx, J. Appl. Phys. **33**, 3078 (1962).